Tellus (2003), 55B, 857–878
Printed in UK. All rights reserved

TELLUS
ISSN 0280–6509

Shipboard measurements of atmospheric oxygen using a vacuum-ultraviolet absorption technique

By BRITTON B. STEPHENS[1]*, RALPH F. KEELING[2] and WILLIAM J. PAPLAWSKY[2], [1]*National Center for Atmospheric Research, Boulder, CO 80307-3000, USA;* [2]*Scripps Institution of Oceanography, University of California, San Diego, La Jolla, CA 92093-0244, USA*

(Manuscript received 15 August 2002; in final form 12 March 2003)

ABSTRACT

We have developed an instrument for making continuous, field-based, part-per-million (ppm) level measurements of atmospheric oxygen concentration, and have implemented it on research cruises in the equatorial Pacific and Southern Oceans. The instrument detects changes in oxygen by the absorption of vacuum ultraviolet (VUV) radiation as it passes through a flowing gas stream, and has a precision comparable to existing laboratory techniques. Here we describe the VUV instrument and present atmospheric O_2 and CO_2 data collected from the NOAA ship Ka'imimoana in the equatorial Pacific during April and May of 1998, and from the NSF ship Lawrence M. Gould in the Southern Ocean during October 1998. These data represent the first field-based measurements of atmospheric O_2, and significant additions to the O_2 datasets in these regions. Our boreal-springtime equatorial measurements reveal significant short-term variations in atmospheric O_2, resulting from variations in atmospheric mixing relative to the strong interhemispheric gradient. Our austral-springtime Southern Ocean observations confirm the low O_2 concentrations seen in flask samples from this region, allow the separate identification of oceanic and industrial influences on CO_2, and provide evidence of a Southern Ocean source for CO_2 at this time of year. These shipboard VUV observations do not provide any evidence to support coupled ocean–atmosphere model predictions of a large decreasing atmospheric O_2 gradient between equatorial and high-southern latitudes.

1. Introduction

The development of an interferometric O_2 measurement technique by Keeling (1988) provided a means of measuring atmospheric O_2 with a precision of a few per meg [see eq. (1)], and first allowed the detection of spatial, seasonal and interannual O_2 variations. More recently, Bender et al. (1994) have demonstrated measurements of a similar precision using a stable-isotope mass spectrometer. The use of these techniques on flask samples collected from a global network of stations has led to new insights into the carbon cycle that were not possible through measurements of CO_2 alone. Most significantly, the detection of interannual trends in O_2 has allowed the partitioning of global oceanic and terrestrial sinks for anthropogenic carbon (Keeling and Shertz, 1992; Bender et al., 1996; Keeling et al., 1996; Battle et al., 2000; IPCC, 2001). Measurements of seasonal cycles in atmospheric O_2 have also provided hemispheric estimates of oceanic biological productivity (Keeling and Shertz, 1992; Bender et al., 1996) and air-sea gas exchange rates (Keeling et al., 1998b). In addition, observed latitudinal variations in atmospheric O_2 constrain the southward transport of O_2 and CO_2 in the oceans (Keeling et al., 1996), and have been used to test the performance of coupled ocean–atmosphere carbon cycle models (Stephens et al., 1998).

The model–observation comparisons made by Stephens et al. (1998) revealed significant discrepancies. However, some of the more extreme model predictions could not be directly tested because of a gap in the sampling network at equatorial latitudes, and

*Corresponding author.
e-mail: stephens@ucar.edu

large, poorly understood, atmospheric O_2 gradients at high southern latitudes. One limitation of the interferometric and mass-spectrometric methods is that the size of the instruments prohibits their field use, which typically limits the spatial and temporal resolution of their measurements to that which is feasible through flask sampling. Field-based measurements from continuous analyzers have the potential to significantly extend the spatial and temporal resolution of existing atmospheric O_2 measurements, thus helping to refine the constraints of Stephens et al. (1998) and promising new insights into biogeochemical cycling on even smaller time and space scales. Manning et al. (1999) have recently developed a paramagnetic analyzer which is well suited for continuous O_2 measurements at remote field-stations. However, this instrument's high degree of motion-sensitivity precludes its use on a moving platform such as a ship or airplane. Other important recently developed techniques include somewhat less-precise but relatively straightforward flask gas-chromatography (Tohjima, 2000) and continuous fuel-cell (Stephens et al., 2001) instruments.

The VUV instrument described here has a precision and a temporal resolution that is comparable to or better than other methods. We report a 1σ precision of 6 per meg [see eq. (1)] for a discrete 10-s measurement, a precision of 1 per meg for a 5-min average, and a reproducibility with other methods to $\pm$ 3 per meg. A moderate motion sensitivity of the instrument resulted in a degradation in the 5-min precision to a typical at-sea value of 2.5 per meg. These extreme levels of precision are a result of establishing a high VUV absorption coefficient, very low-noise amplification of the consequently small photocathode signals, and rapid switching between sample and reference gases. The external reproducibility of atmospheric O_2 measurements depends critically on careful gas handling to eliminate potential sources of fractionation (Keeling et al., 1998a; Stephens, 1999). We describe the VUV analyzer in detail in section 2 below.

This instrument is particularly fit for improving upon the spatial and temporal resolution of existing flask measurements, specifically by filling in gaps in the meridional atmospheric O_2 gradient and improving our understanding of high-frequency atmospheric O_2 variability. With these goals in mind, we have successfully implemented the VUV instrument on ships in the equatorial Pacific and the Southern Ocean. We have also used this instrument to measure atmospheric O_2 variations for a month during summer at Harvard Forest, Massachusetts. In section 3 we present results obtained aboard the NOAA ship Ka'imimoana between 18 April and 20 May 1998, along 125° and 140°W in the eastern equatorial Pacific. We discuss sources for the observed O_2 variability, which on short timescales appears to be dominated by sampling across the strong interhemispheric O_2 gradient. The mean O_2 concentration observed during this cruise may also have been sensitive to relatively high dissolved O_2 concentrations associated with the strong El Niño event at this time. In section 4 we present results obtained aboard the NSF ship Lawrence M. Gould between 2 and 8 October 1998, during a transit of Drake Passage in the Southern Ocean. We are able to distinguish oceanic and industrial influences on our observations, and discuss their implications for Southern Ocean CO_2 fluxes at this time of year. We also present a theory to explain the high annual-mean O_2 concentrations observed in South Pole flask samples through a covariance of atmospheric transport and air–sea fluxes. Finally, in section 5 we compare our equatorial and high-southern latitude measurements and consider what information they and future measurements may contain about the southward transport of O_2 and CO_2 in the oceans.

2. Vacuum ultraviolet O_2 analyzer

2.1. Instrument theory

Ultraviolet radiation in the band 10–200 nm is strongly absorbed by atmospheric O_2, and thus is typically only observable in the presence of a vacuum. This "vacuum" ultraviolet was first used to measure atmospheric O_2 concentrations over 30 yr ago (Kaplan et al., 1971). However, there have been few improvements to the technique since then (Wong, 1978; Kronick et al., 1980; Wong, 1986), and its demonstrated precision is much coarser than the geochemically interesting variations of ~0.0001%. Because of the high O_2 concentration in the atmosphere of 21%, ppm-level variations in O_2 mole fraction are much more difficult to measure than for trace gases. To accommodate these small signals, and to provide a framework that is insensitive to the diluting affects of CO_2, variations in atmospheric O_2 are commonly expressed as deviations in the O_2/N_2 ratio relative to a reference, where

$$\delta(O_2/N_2)\,(\text{per meg}) = \left(\frac{(O_2/N_2)_{\text{sample}}}{(O_2/N_2)_{\text{reference}}} - 1\right) \times 10^6. \quad (1)$$

In these units, the addition of 1 μmol of O_2 to 1 mol of dry air increases $\delta(O_2/N_2)$ by 4.8 per meg (Keeling et al., 1998a). While mass spectrometers measure the O_2/N_2 ratio directly, interferometric, paramagnetic, gas-chromatographic, fuel-cell and optical instruments all measure signals more directly related to the mole fraction of O_2, which is also sensitive to variations in other gases. It is thus necessary to simultaneously measure and make a correction for variations in CO_2 (Keeling et al., 1998a), and to dry the sample air to very low or constant H_2O concentrations. In addition to the effect of dilution, CO_2 has an additional interference effect on the VUV measurement. Natural variations in argon and other species are small enough that they can be ignored in most applications.

Observed variations in atmospheric oxygen include interannual trends of around -15 per meg yr^{-1}, interhemispheric differences of around 30 per meg, and seasonal cycle amplitudes of up to 100 per meg (Keeling et al., 1993). To resolve these features, and to distinguish terrestrial and oceanic influences by comparison to CO_2 data, one must be able to measure O_2 at a precision of a few per meg. Consequently, any viable detection system must be sensitive to variations in O_2, and free of noise, at a relative level close to one ppm. The absorption of ultraviolet radiation is well suited to this task, as light sources can be made stable, light levels can be measured and signals amplified, and pressure in a flowing gas stream can be maintained, all at the ppm level.

The analyzer that we have developed measures the absorption of VUV radiation as it passes through a flowing air stream (Kaplan et al., 1971). For a light source, we use a radio-frequency (RF) powered xenon lamp, which has a strong emission line in the Schumann–Runge continuum at 147 nm (Samson, 1967). Because O_2 is the primary atmospheric absorber at 147 nm, variations in absorption are related to the O_2 mole fraction (X_{O_2}) via the Beer–Lambert law:

$$I = I_0 \exp\left(-k\ell P \frac{T_0}{T} X_{O_2}\right)$$
$$\text{or } I = I_0\, e^{-\alpha} \tag{2}$$

which can also be expressed in differential form as

$$\frac{\Delta I}{I} = -\alpha\left(\frac{\Delta X_{O_2}}{X_{O_2}}\right) \tag{3}$$

where I_0 is the original light intensity, I is the transmitted light intensity, α is the sensitivity, $k \approx 320$ atm^{-1} cm^{-1} (Watanabe et al., 1953) is the absorption coefficient of O_2 at 1 atm, ℓ is the path length, P is the air pressure, T is the air temperature, and $T_0 = 273.15$ K. Equation (3) indicates that the response of the instrument to small changes in X_{O_2} will be linear. For O_2 absorption at 147 nm, departures from linearity over the natural range of variability are expected to be less than 0.1 per meg. Published data indicate a CO_2 absorption coefficient at 147 nm that is approximately 5% of that for O_2 (Inn et al., 1953; Watanabe et al., 1953). We have conducted independent measurements using the VUV instrument, which give a value of 4.7% [see eq. (4)].

To achieve the desired instrument sensitivity, it is necessary to use a path length and pressure corresponding to optically thick conditions. However, there is a trade off with inherent noise at the resultantly low detector currents. For the photocathodes we employ, the maximum allowable current of 100 nA corresponds to an inherent shot-noise limit of 2.8 per meg for a 0.2 s measurement. Under ideal conditions, we have verified that our lamp, detection and amplification circuitry, and steady-state flow-control are capable of performing at this limit (Stephens, 1999). As discussed below, lower-frequency noise, using an open rather than a sealed lamp, flow perturbations from switching between sample and standard gases, and motion sensitivity all lead to a somewhat less precise field measurement.

2.2. *Instrument design*

To overcome difficulties in constructing sealed xenon lamps with sufficient lifetimes, we used a flow-through lamp design. Although we have more recently tested a commercially available sealed lamp with a suitable lifetime and lower noise, the data presented here were collected using our original open lamp. Figure 1a is a schematic of the gas handling and power supply configuration of the open xenon lamp. The lamp body consists of a 3″ long by 1/2″ diameter Pyrex tube fused to a sapphire window at one end, with two perpendicular 1/4″ arms at the other end (Glass Contour, Laguna Beach, CA). To maintain a constant xenon pressure and flow, we bleed xenon from a 250 mL volume at ∼15 psi, as measured by a pressure gauge (P), through a crimped capillary and into the lamp. A vacuum pump downstream of a needle valve pulls xenon from the lamp. We adjust this downstream needle valve so that the lamp pressure is ∼0.3 Torr. The

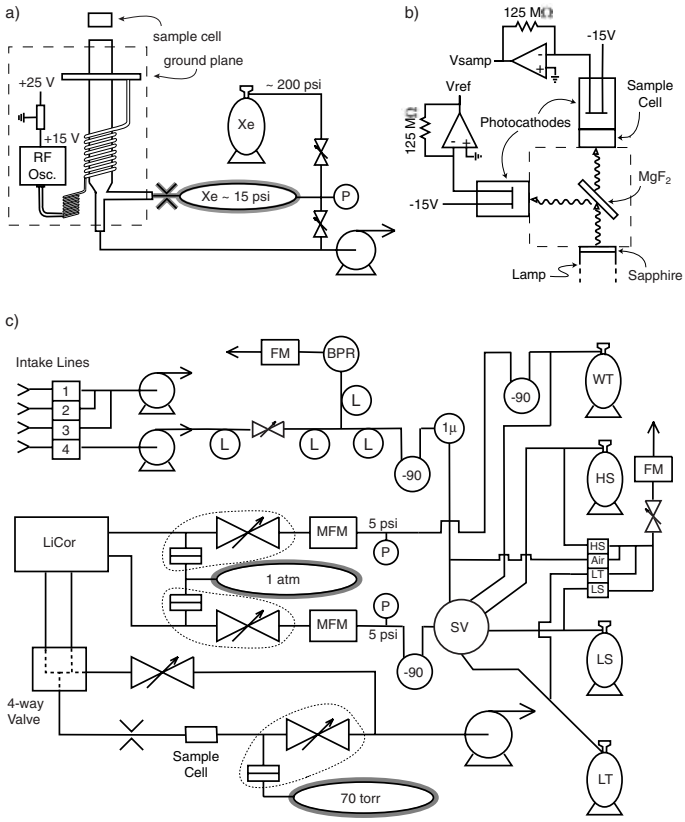

Fig. 1. (a) Xenon lamp gas-handling and power-supply schematic. The dashed line represents a $1/4''$ wall aluminum enclosure. (b) Optical and electronic signal-detection schematic. The dashed line represents an evacuated volume. (c) Gas handling schematic. Dotted loops enclose linked differential pressure gauges and feedback control valves. Grey shading in (a) and (c) represents foam insulation. The sample cell is illustrated in all three panels. See text for a complete description of the components and the flow and pressure balancing scheme.

capillary has a conductance such that the throughflow of xenon is ∼0.02 mL STP min^{-1} at these pressures, corresponding to a flushing time of ∼10 s. Although the lamp output does exhibit a long-term drift resulting from the decreasing upstream xenon pressure, this is effectively removed by the switching and calibration scheme, and the upstream volume can be occasionally refilled with xenon from a high-pressure cylinder. It is necessary to insulate this volume and the capillary to avoid short-term lamp variability in response to temperature changes.

Figure 1a also illustrates the power supply for the lamp, which consists of a 15 W, 180 MHz RF oscillator (LCF Enterprises, Camarillo, CA) coupled to the lamp via a double coil of copper magnet wire. This double coil is connected between the RF oscillator output and a ground plate. To avoid potential problems of window degradation, we positioned the ground plate $2''$ from the lamp window to limit the forward advance of the plasma. We supply power to the RF oscillator from a 25 VDC power supply coupled to a 15 VDC voltage regulator. The lamp and RF oscillator are enclosed in an aluminium box that shields other instrument components from RF interference. This box has $1/4''$ thick walls, which provide adequate thermal inertia to the system without further insulation. An uncoated magnesium fluoride window (Fig. 1b) passes a fraction of the lamp output through a sample cell and then onto a detector, while reflecting the rest of the output directly onto a reference photocathode. This beamsplitter and extra detector were included so that fluctuations in the lamp output could be removed by comparing the

sample and reference signals. In practice, however, the RF lamp variability was small enough that this second photocathode was only useful in identifying occasional anomalous spikes in lamp output.

Figure 1b is a schematic of the optical and electrical configuration of the signal detection assembly. We use solar-blind cesium iodide photocathodes (Hamamatsu Corporation, Bridgewater, NJ) as detectors. These photocathodes are only sensitive to wavelengths between 110 and 220 nm and have a quantum efficiency of approximately 1% at 147 nm. The wavelength of the transmitted light is further constrained by the sapphire window on the lamp that effectively cuts out wavelengths shorter than 140 nm, including a secondary xenon line at 130 nm. At the operating sample-cell pressure, the photocathode currents are approximately 50 nA. We use the feedback ammeter circuits shown in Fig. 1b to convert this signal to ~6 V, which we measure using a 6 1/2 digit voltmeter. The low-noise op-amp (AD549LH) and the low temperature coefficient (5 ppm K^{-1}) of the 125 MΩ feedback resistor (Caddock Electronics, Riverside, CA) are critical in this design.

The above components are all only stable to a ppm on relatively short timescales. Because of this, the instrument must rapidly switch between the sample and a reference gas to compensate for inherent signal drift, while at the same time maintaining pressure and flows in the sample cell constant to 1 ppm. Precision improves with shorter and shorter switching times, but pressure control eventually becomes too difficult and a higher fraction of signal is lost during the transitions. In consideration of these issues, we selected a switching time of 5 s. This time period was not rigorously optimized, and recent tests have shown improved performance when switching every 3 s. The gas handling system must also provide for the cryogenic drying of air, for the automatic selection of multiple sample and calibration gases, and for greater flow rates through sample intake tubes than through the instrument, all without producing any fractionation or transient surface effects. Figure 1c is a schematic of the gas handling system that we have designed to accomplish these tasks.

An absolute requirement for O_2 measurement stability is that all points in the gas handling system experience constant flow rates with unchanging pressure and moisture characteristics. This arrangement prevents transient surface adsorption–desorption effects, and the aliasing of diffusive O_2/N_2 gradients that form across temperature, pressure and humidity gradients such as through a cold trap or a needle valve (Keeling et al., 1998a). A diaphragm pump (Fig. 1c) pulls sample air at 2 L min^{-1} through multiple inlet lines, such as from the bow and stern of a ship or multiple heights in a forest. A set of solenoid valves selects air from one of these lines, which is delivered to the instrument by a second diaphragm pump.

Desired field response times often require that gases be pulled through the intake lines at a rate much faster than that used by the instrument. To accommodate these rapid flows, a tee dumps most of the inlet gas out through a back-pressure regulator (BPR) and flowmeter (FM), and sends only 80 mL min^{-1} through the analyzer. Back-pressure regulators fractionate O_2 relative to N_2, so we put a 2 m loop (L) of 1/4″ tubing between the tee and the regulator to insure that any gradients resulting from this fractionation do not influence the small flow going to the analyzer. Manning (2001) has demonstrated that the combination of a tee and pump-induced air pulsations also fractionates O_2 relative to N_2. As shown in Fig. 1c, there are two additional 2 m coils of 1/4″ tubing and a needle valve between the diaphragm pump and the tee to minimize the magnitude of the air pulsations at the tee and to limit the intake flow rate to 2 L min^{-1}. Without this additional tubing and valve, the tee can fractionate O_2/N_2 by as much as 70 per meg, whereas with them any fractionation appears to be less than 3 per meg (see Fig. 4 and discussion in Section 3 below).

After this tee, the sample air passes through a preliminary cold trap, maintained at either −78 °C by dry ice or −90 °C by a cryogenic chiller, and then through a 1.0 μm filter to remove any remaining particles. A rotary selector valve (SV) chooses between this sample air and several calibration gases (HS, LS, LT). Immediately upstream of this valve, each calibration line is connected to a purge line and solenoid valve to allow flushing of the lines and regulators prior to their delivery of air to the detector. The selected air stream is passed through a second cold trap and a mass-flowmeter (MFM) before reaching the first active flow control assembly (Fig. 1c). A separate cylinder of reference gas, called the working tank (WT), continuously delivers air through another cold trap and mass-flowmeter to a second flow control assembly. The back-pressure regulator and the reference cylinder regulators are set so that these two gas streams are at a pressure of 5 psig. This pressure then drops to ~1 atm as the gases pass through a pair of automatic needle valves that are adjusted by feedback flow controllers (MKS, Andover, MA). These flow controllers

are referenced to 10-Torr full-scale differential pressure gauges (MKS) that measure the difference in pressure between the sample lines and a pressure-reference volume held at ~1 atm.

The sample or calibration gas and the WT gas next pass through the sample and reference cells, respectively, of a non-dispersive infrared (NDIR) CO_2 analyzer (LiCor, Lincoln, NE). These two gas streams are then pulled by a rotary-vane vacuum pump through a pneumatic four-way valve (Micromass Ltd., UK). This valve directs one stream through the sample cell and the other through a bypass loop. A third pressure-reference, feedback-controller assembly adjusts a downstream needle valve to hold the sample cell pressure at 70 Torr, while a manual needle valve on the bypass loop can be adjusted to match the flows. This feedback assembly uses a 1-Torr full-scale differential pressure gauge (MKS) that allows short-term control to better than 10^{-4} Torr. The 70 Torr cell pressure and 3 mm path length correspond to an instrument sensitivity α of approximately 1.6 ppm-signal (per meg $O_2)^{-1}$. The two pressure-reference volumes (Fig. 1c), at 1 atm and 70 Torr, are insulated against short-term temperature fluctuations.

2.3. *Instrument performance*

Figure 2a shows the VUV signal while switching every 5 s between WT and sample air while on land. The small internal volume and rapid switching capability of the four-way valve are essential to the fast recovery times shown in this figure. This valve must also be able to endure over 17 000 switches per day. The 100-ppm spikes at the end of each step correspond to a temporary drop in cell pressure resulting from the switching of the four-way valve. The residence time of the gas in the sample cell is 0.2 s. To allow for pressure equilibration and sweepout of the sample cell, we reject the first three 0.2 s integrations after each switch. The instrument sensitivity and the measured CO_2 concentrations determine the conversion from the relative signal units shown in Fig. 2 to units of per meg. The sample gas during the period shown in Fig. 2a had an O_2/N_2 ratio that was around 100 per meg greater than the WT value. The overall downward trend in Fig. 2a is an example of the type of lamp and detector variability that is compensated by the 5-s switching.

As the basis of the O_2 measurement, we use the measured difference between successive 5-s analyses, such as those shown in Fig. 2a. By comparing two reference gases, we estimate a 1σ error on one 10-s measurement (differencing two 5-s averages) of 6 per meg, while averaging these differences over 5-min periods results in a precision of 1 per meg. Figure 2b shows an example of these 5-s differences, measured over 2 h while on the Lawrence M. Gould in calm conditions. To determine actual oxygen concentrations, it is necessary to compare the differences between a sample

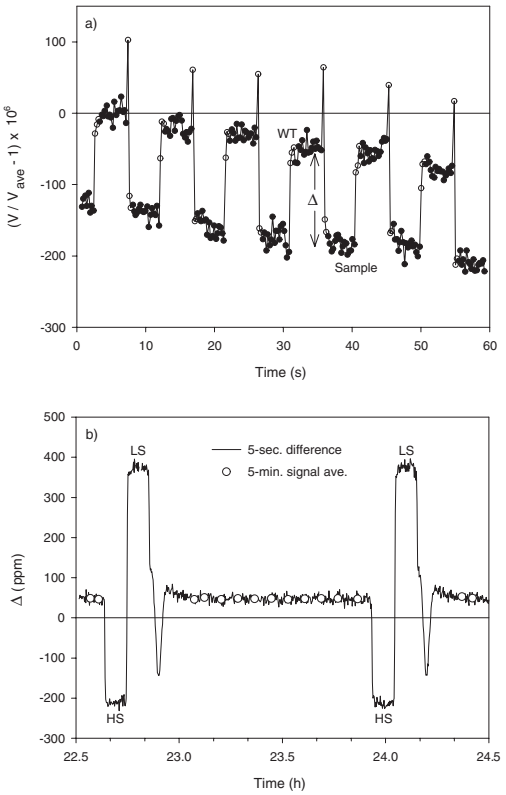

Fig. 2. Sample data from VUV analyzer. (a) Signals from 5-s switching between working tank (WT) and sample gas on land. Values are plotted in V relative to the average signal for the first WT jog, and are inversely related to concentration. Hollow symbols represent the first three points after each switch that are discarded in the standard data-workup program. (b) Sample–WT differences over an hourly measurement cycle from Lawrence M. Gould during calm conditions. Values are plotted as the relative difference between successive 5-s analyses in units of ppm. Sequence is 7 min of high span (HS), 7 min of low span (LS), and 66 min of sample gas. Circles represent 5-min averages. The dip in the O_2 signal after the LS-sample switch results from the rotary valve passing the HS port on its way to the sample port.

and reference gas to those between the same reference gas and other known standards. In addition to the WT gas, we use high-span (HS) and low-span (LS) calibration gases which have O_2/N_2 ratios approximately 200 per meg higher and lower than ambient air. We determine the O_2/N_2 ratio in these reference gases to approximately ± 1 per meg by repeated measurements on the Scripps O_2 Laboratory interferometer (Keeling, 1988; Keeling et al., 1998a). Once during every 80 min of measurement (Fig. 2b) we analyze these gases for 7 min each. For 5 min prior to introducing these gases to the detector, we purge their lines and regulators at a flow rate of 300 mL min^{-1}. We then reject the first 3.5 min of data after switching gas lines, and calculate HS and LS signal values using the last 3.5 min.

Because the rotary selector valve must pass by another calibration gas port to get back to the sample air position, it takes longer for the signal to restabilize (Fig. 2b). Consequently, we reject the first 7 min of sample signal after this switch. To calculate O_2/N_2 ratios over the 60 min of usable sample signal, we initially compare the sample and calibration signals on the basis of changes in apparent O_2 mole fraction at constant CO_2. To convert from deviations in apparent mole fraction to deviations in per meg, it is necessarily to use the NDIR signal to calculate the CO_2 concentration, and then to apply CO_2 dilution and interference corrections (Keeling et al., 1998a):

$$\delta(O_2/N_2) = \frac{\delta X_{O_2} + ([CO_2] - 363.29) \times (X_{O_2} - 0.047)}{X_{O_2}(1 - X_{O_2})} \quad (4)$$

where $[CO_2]$ is the calculated CO_2 concentration in μmol mol^{-1} for the sample gas and 363.29 is the average CO_2 concentration of the reference cylinders defining zero on the Scripps O_2/N_2 scale. Multiplying the deviation in CO_2 by X_{O2} corrects for the diluting effect of CO_2 on the apparent mole fraction, and multiplying the deviation by -0.047 corrects for the CO_2 interference effect intrinsic to the VUV measurement.

The primary challenge to using the VUV instrument on a ship was its motion sensitivity. In theory, an optical instrument can be designed to be very insensitive to motion. In practice a number of effects, including the motion sensitivity of the differential pressure gauges and proportional solenoid valves, and small motions in the RF coil and plasma geometry can contribute additional noise to shipboard VUV measurements. Recent tests have indicated that the largest source of instrument noise during these cruises resulted from incomplete shielding of the RF radiation, which allowed small motions of the lamp box relative to the instrument rack and nearby metal objects to affect the tune of the RF coil. Occasionally during the cruises discussed below, the conditions at sea were calm enough that the instrument performed as well as it did in the laboratory. For example, the 5-min averages shown in Fig. 2b have a standard deviation of 1.1 per meg. However, this was not always the case. The increase in short-term signal variability associated with 2–3 m seas corresponded to an increase in the 1σ error on 5-s differences to 10 per meg O_2, and on 5-min averages to 2.5 per meg (Stephens, 1999).

For 1 h during every day of measurement, we analyze a fourth calibration gas. This long-term reference (LT) gas provides a daily check of the measurement stability, it allows direct comparisons between measurements made in different environments and using different HS and LS cylinders, and it provides a means of estimating the precision of hourly measurements. The statistical error associated with summing 12 5-min means to get an hourly value is rather small, but this does not account for signal drift on time scales between 5 min and 1 h. Based on 25 at-sea measurements, the average difference between the VUV and interferometer LT values was 0.7 ± 2.2 per meg (Stephens, 1999), and we use this 1σ error as our estimated precision on the hourly data presented below. We also collected shipboard flask samples for analysis on the interferometer and comparison with adjacent VUV measurements. Excluding one outlier, the average difference for nine flask samples was 0.4 ± 2.8 per meg (Stephens, 1999). This further demonstrates the external reproducibility, as well as the linearity of the VUV measurements.

For the ancillary CO_2 measurements, we use the same calibration scheme as for O_2 with several exceptions. Because rapid switching is not necessary for CO_2, the NDIR analyzer is upstream of the four-way valve and we use 10-s average signals instead of 5-s differences as the base measurement. Also, the NDIR signal is not linear with CO_2 concentration. We have used a quadratic fit to four reference gases as a calibration curve. In comparison with laboratory measurements, we obtain a CO_2 precision of 0.05 ppm and an external reproducibility of 0.3 ppm.

3. Shipboard measurements in the equatorial pacific

The equatorial Pacific is an important region for both the long-term balance and the interannual variability of atmospheric CO_2 (Le Quéré et al., 2000). Furthermore, the biological, thermal and dynamic processes that affect air–sea CO_2 fluxes in this region are closely linked to air–sea O_2 fluxes (Wanninkhof et al., 1995), which may be easier to detect. For example, the upwelling of DIC and preformed nutrients, and the strong air–sea heat fluxes, lead to a net outgassing of O_2 and CO_2 from the equatorial Pacific. While the atmospheric imprint of this CO_2 outgassing is spread out in time and space owing to its buffering chemistry and relatively high solubility in surface waters, the more rapid O_2 outgassing may lead to very large atmospheric signals. The coupled atmosphere–ocean models examined by Stephens et al. (1998) predict annual-mean atmospheric O_2 peaks on the order of 10 per meg between 20°N and 20°S. These models also predict that the equatorial Pacific is a region of significant temporal and spatial variation in atmospheric O_2. Unfortunately, these model predictions can not currently be tested, nor the extent of equatorial O_2 outgassing be measured, because of gaps in the flask sampling networks (Keeling et al., 1996; Bender et al., 1994). Bender et al. have a very promising program of flask collection from commercial and research ships in the Pacific; however, because of high natural variability and unpredictable shipping changes, these measurements have not yet been used to address this question. The measurements presented here represent a complimentary step toward filling this equatorial data gap, and provide direct evidence of the controls on low-latitude atmospheric O_2 over a range of time and space scales.

We have used the VUV instrument to measure atmospheric O_2 in the eastern equatorial Pacific, aboard the NOAA ship Ka'imimoana. This ship is dedicated to servicing the Tropical Atmosphere Ocean (TAO) array of moored buoys, and thus provides an excellent platform for conducting repeatable geochemical surveys of this region. The data presented here are from leg GP2-98, which departed San Diego on 18 April 1998. This cruise included maintenance along the 125°W buoy line, recovery of a drifting buoy at 3°N, 147°W, and maintenance along the 145°W buoy line before returning to Honolulu on 20 May (Fig. 3). The two southernmost turnaround points were within or just

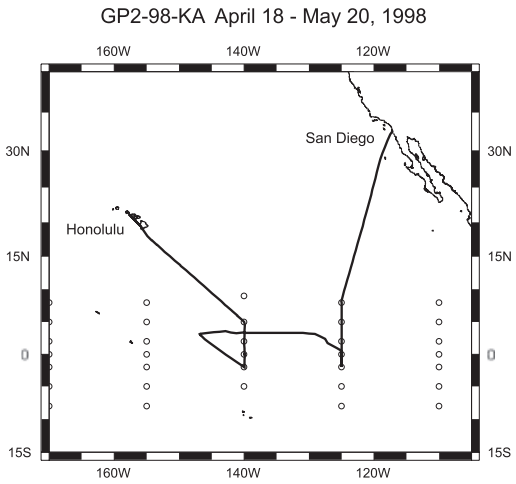

Fig. 3. Map showing the cruise track for Ka'imimoana leg GP2-98. The circles represent the locations of the TAO array buoys at the time of the cruise.

south of the Intertropical Convergence Zone (ITCZ). Both the position of the ship relative to the ITCZ at these times and the latitudinal history of the sampled air during the rest of the cruise had significant consequences for the measured O_2 concentrations.

The VUV O_2 and infrared CO_2 instruments analyzed air drawn from one of two sample lines: on a bow mast approximately 20 m above the water and at a high point on the aft control tower approximately 15 m above the water. We manually switched between the fore and aft sample lines according to the prevailing winds to avoid sampling air from the engine exhaust stacks located amidships. However, it was still necessary to filter the data for times when exhaust air did occasionally get in the sample lines, which were easily identifiable by rapid O_2 and CO_2 excursions. We show the resulting O_2 and CO_2 data, averaged over hourly periods and plotted versus time, in Fig. 4. We express oxygen values in the figures and table relative to the Scripps O_2/N_2 scale.

During the first week of measurements, we discovered that the back-pressure regulator tee was fractionating O_2 relative to N_2 by approximately 68 per meg, and that this fractionation was sensitive to flow and pressure variations at the back-pressure regulator. We succeeded in eliminating this fractionation by reducing the intake flow rate from 6 to 2 L min^{-1} and minimizing flow pulsations at the tee by adding the needle-valve constriction and three loops of tubing shown between

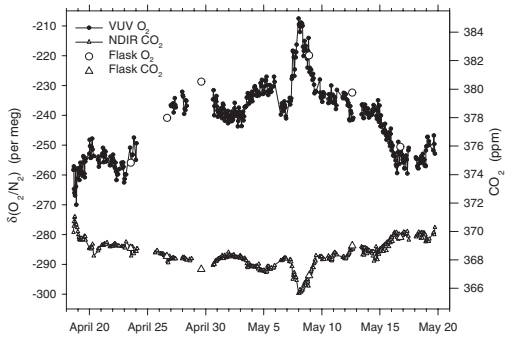

Fig. 4. Hourly-mean concentrations of atmospheric O_2 and CO_2 from GP2-98-KA. The vertical axes are scaled to be equivalent on a molar basis. The ticks on the *x*-axis correspond to midnight local time and are labeled with the date of the following day. The large symbols represent 5-L flask samples collected aboard the ship and analyzed on the Scripps interferometer. The O_2 values were determined as described in section 2 from data similar to that in Fig. 2. After 30 April, the O_2 values have an uncertainty of ± 3 per meg. Prior to 30 April, the O_2 values have been shifted down by 68 per meg to account for an independently quantified fractionation effect and consequently have a higher uncertainty of ± 10 per meg (see text). The data gaps around 25 and 29 April correspond to periods of instrument modification and testing to address this effect. The uncertainty of the CO_2 measurements is $\pm$ 0.3 ppm.

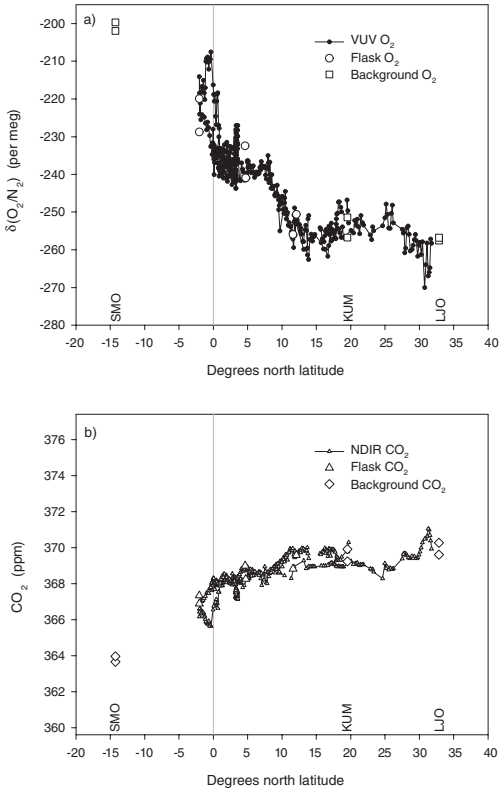

Fig. 5. Hourly-mean shipboard O_2 and CO_2 plotted versus latitude from GP2-98-KA. Data are the same as in Fig. 4 for (a) O_2 concentrations and (b) CO_2 concentrations. The large squares and diamonds represent measurements on flask trios collected on 23 April and 6 May at La Jolla (LJO), on 4 and 19 May at Samoa Observatory (SMO), and on 12 and 26 May at Cape Kumukahi (KUM).

the intake pump and cold trap in Fig. 1c. We verified the lack of fractionation by finding an insensitivity of the measurements to flow and pressure variations at the back-pressure regulator, and quantified the effect to within $\pm$ 10 per meg by repeatedly changing between the new and old configurations. We have adjusted the O_2 data before 30 April to account for these effects and allow for an additional amount of uncertainty in our reported accuracy during this time (Fig. 4).

The large symbols in Fig. 4 represent six 5-L flask samples that we collected on the ship, and analyzed on the Scripps O_2 Laboratory interferometer. The flask sample taken on 12 May is 8 per meg higher than the adjacent VUV O_2 values. However, because the O_2:CO_2 ratio in this flask sample is also anomalous (see Fig. 6 later), it is likely that a problem during flask collection or storage, rather than VUV instrument error, is the cause of this discrepancy. The other three flasks that overlap VUV data give O_2 values that are in good agreement with the *in situ* measurements, and do not reveal any consistent offsets. The differences of $\pm$ 2–3 per meg are within the combined errors for these two techniques. One of these flasks overlaps the early fractionation-adjusted VUV data; however, we calculated this adjustment independent of the flask result. The two flask samples taken when continuous data are not available give O_2 values that appear reasonable in comparison to the nearby VUV data and trends.

Figure 5 shows the same continuous data plotted versus latitude. Together, Figs. 4 and 5 show coherent O_2 variations on timescales of hours to weeks and space scales of tens to hundreds of kilometres. For the first several days steaming south from San Diego, O_2 concentrations increased by $\sim$10 per meg and CO_2 concentrations decreased by $\sim$2 ppm. However, at around 25°N these trends shifted as CO_2 leveled off and O_2 began a slight decrease (Fig. 5). Then, on the morning of 23 April near 14°N, these trends underwent

another larger shift as O_2 concentrations began a steady climb, and CO_2 a steady decline, that continued all the way to the Equator. On the first pass across the Equator along 125°W, O_2 concentrations increased by a total of ∼10 per meg and CO_2 decreased by ∼1 ppm as indicated by the flask sample taken at 2°S on April 29 (Fig. 4). We observed a much larger jump across the Equator on the second pass just over a week later and 15° further west, when O_2 increased by ∼30 per meg and CO_2 decreased by ∼3 ppm. These concentration excursions along 145°W longitude actually diminished by a factor of 2 by the time the ship reached its southernmost point at 2°S. From this point to the end of the cruise in Honolulu, we observed the reverse of the general trends seen earlier from San Diego to the Equator. Again at around 14°N we observed a leveling-off of the CO_2 trend and a shift to slightly increasing O_2 concentrations.

The overall latitudinal gradients shown in Fig. 5 are consistent with the larger-scale interhemispheric differences in O_2 and CO_2 at this time of year. We have also included points in this figure representing background-station flask trios collected near the beginning of the cruise at La Jolla, California (LJO), near the middle of the cruise at American Samoa (SMO), and near the end of the cruise at Cape Kumukahi, Hawaii (KUM) as part of the Scripps O_2 Laboratory sampling program. The LJO and KUM measurements agree well with the adjacent continuous values, and the southward trends are generally in line with the SMO concentrations at 14°S. While the interhemispheric O_2 and CO_2 gradients reverse every summer and winter, this cruise happened to take place at the time of year with the greatest interhemispheric O_2 and CO_2 differences.

The observed latitudinal CO_2 gradient resulted from a combination of terrestrial respiration occurring during the boreal winter preceding this cruise and the large industrial source in the northern hemisphere. The observed latitudinal O_2 gradient was oppositely affected by the corresponding industrial and terrestrial O_2 sinks in the north. In addition, the O_2 gradient was steepened by oceanic outgassing in the southern hemisphere resulting from net productivity, and by oceanic ingassing in the northern hemisphere resulting from enhanced vertical mixing of O_2-depleted waters, which occurred during the boreal winter. An indication of the relative terrestrial and oceanic contributions to the latitudinal gradients presented here can be obtained by directly comparing the O_2 and CO_2 data. Figure 6a shows a plot of the observed O_2 versus CO_2 concentrations. These data correlate well, with an average

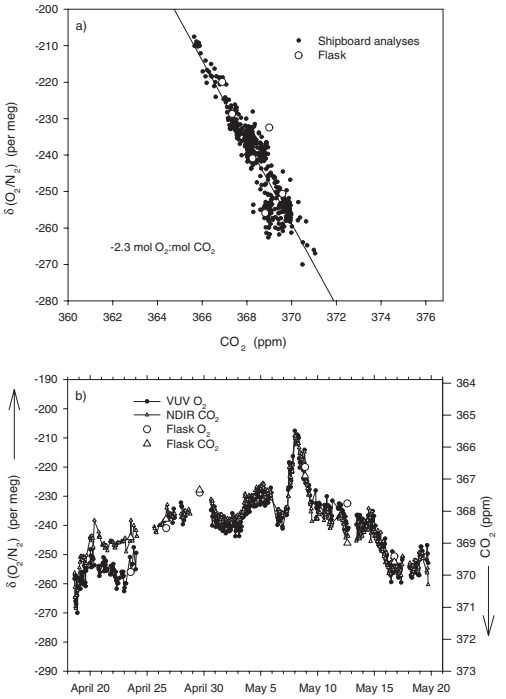

Fig. 6. (a) Hourly-mean and flask O_2 versus CO_2 concentrations from GP2-98-KA. The line and reported slope are from a least-squares fit to the VUV data. The axes are scaled to be equivalent on a molar basis. (b) Hourly-mean and flask O_2 and scaled CO_2 data. Same as Fig. 4, but with the CO_2 axis flipped and scaled by −2.3 mol O_2:mol CO_2.

slope of −2.3 mol O_2:mol CO_2. By comparison, fossil fuel burning alone would produce a slope of around −1.4 mol O_2:mol CO_2 (Keeling, 1988), and terrestrial exchange would produce a slope of around −1.1 mol O_2:mol CO_2 (Keeling, 1988; Severinghaus, 1995). The more negative observed slope reflects the influence of oceanic O_2 exchange, which has very little corresponding CO_2 flux. The value of −2.3 mol O_2:mol CO_2 is consistent with approximately equal oceanic and terrestrial influences on the interhemispheric O_2 gradient at this time.

The tight relationship between the shipboard O_2 and CO_2 observations is further illustrated in Fig. 6b. The one time when O_2 did not closely track CO_2 at a consistent ratio is from 20 to 23 April, as the ship steamed from 25°N to 13°N near 120°W longitude. During this period, O_2 dropped by ∼10 per meg while CO_2 remained fairly constant. Although instrument error must be considered for this period

of known fractionation problems, the O_2 values determined from the adjusted VUV signal on 23 April are very close to the independently determined flask concentration. An alternative explanation is that this O_2 divergence represents the influence of northern oceanic O_2 uptake. The lower O_2 and higher CO_2 concentrations at the beginning and end of the cruise are, as expected, associated with sampling air from further north. Back trajectories (Stephens, 1999; Draxler and Hess, 1998) show that during the period of anomalous O_2:CO_2 ratios the sampled air was traveling from even further north along the coast of California. The northern Pacific and California coast are both regions of relatively strong vertical mixing at this time of year, which delivers a greater O_2-deficit to the surface than local productivity can compensate. The resulting O_2 uptake in these regions might explain the observed drop in O_2 with constant CO_2 during this period.

Back-trajectory and meteorological analyses also show that variations in the origin of the sampled air, both interhemispheric and between different regions of the eastern Pacific basin, had a significant impact on the measured O_2 and CO_2 concentrations. Figure 7 shows the VUV O_2 data of Fig. 4 along with concurrent measurements of wind speed, wind direction, northward wind component (v), air temperature and relative humidity. As this figure shows, the air sampled near the Equator was primarily delivered by the northeasterly trades, with a few exceptions at the southern extensions of the cruise track. By the turnaround point at 2°S, 125°W, where only a flask sample is available, the winds had shifted to a northwesterly direction. This point also appears to have been a temporal peak in O_2 (Fig. 4). Satellite imagery (Stephens, 1999; NOAA-GOES project) indicates that the ITCZ was relatively indistinct at this time. However, the ship was directly under a thin line of high clouds that did exist, suggesting that it was sampling a convergent mixture of northern and southern air (Stephens, 1999; Draxler and Hess, 1998). On the return back across the Equator, the winds shifted back to the northeast and O_2 decreased (Fig. 7). During the transect to capture the drifting buoy, the ship's latitude remained relatively constant, yet on 3 May we observed a 10 per meg and −1 ppm step in O_2 and CO_2, respectively. Back trajectories for this longitudinal transect (Stephens, 1999) indicate that the observed concentration shifts correspond to a change in the origin of the air from the northeast to the east. At the end of this transect on 6 May, before the ship turned to the south, the winds increased in speed and returned to the northeast, while O_2 and CO_2 returned to values close to those observed 20° to the west (Fig. 7). Variations in the efficiency of atmospheric transport from the north appears to have produced these changes in the observed concentrations, with more efficient southward transport corresponding to low O_2 and high CO_2.

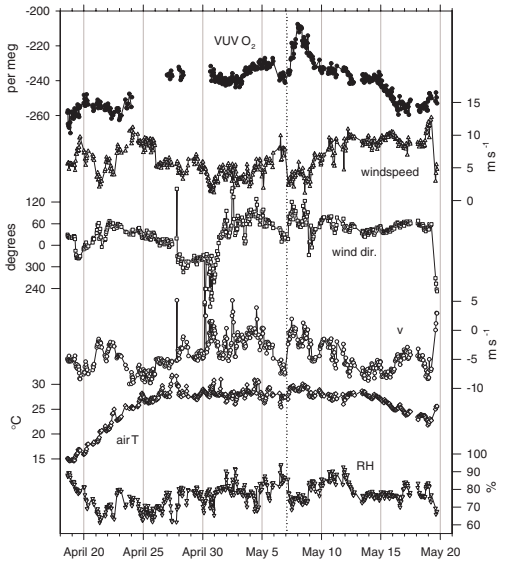

Fig. 7. Hourly-mean shipboard meteorological data from GP2-98-KA. The VUV O_2 data are the same as in Fig. 4. This plot also includes wind speed, wind direction, northward wind component (v), air temperature, and relative humidity (RH). Vertical reference lines are plotted every 5 d at local midnight, and at 0112 local time on 7 May.

The sharpest observed change in O_2 and CO_2 occurred on 7 May, when O_2 jumped by 30 per meg and CO_2 dipped by 3 ppm, as the ship headed south across the Equator. This change was coincident with a sharp slackening of the winds, a shift to a less northerly wind direction, a decrease in relative humidity, an increase in air temperature and a change from almost complete cloud cover to mostly clear skies (Fig. 7). Satellite imagery (Stephens, 1999; NOAA-GOES project) shows that the ITCZ was fairly distinct at this time, and that the ship had just penetrated south of a main line of high clouds centered near 5°N. The ship remained under the patch of clear sky between this and a southern branch of clouds throughout most of 8 May. The O_2 and CO_2 concentrations observed aboard the ship on this day are close to those from a flask sample taken on 5 May

at SMO (Fig. 5), suggesting that the ship was in fact sampling air primarily of southern hemisphere origin. The lack of clouds could indicate descending air conditions, and it is possible that the high-O_2, low-CO_2 air moved north at a higher altitude before descending upon the ship.

At the turnaround point of 2°S, 140°W, the O_2 and CO_2 concentrations were again closer to their more northerly values (Fig. 5). By the time the ship reached this point, the winds had shifted back to the north, relative humidity and cloud cover had increased, and temperature had decreased (Fig. 7). This combination of meteorological observations suggest that the O_2 and CO_2 concentrations observed near the Equator were highly sensitive to the position of the ship relative to the ITCZ and local synoptic weather systems. In comparison to the short-term variations of up to 30 per meg that we observed, the seasonal-cycle amplitude (Keeling et al., 1998b) and interannual trends (Keeling et al., 1996) at MLO are only 13 per meg and 15 per meg yr^{-1}, respectively. Manning and Keeling (1994) found that the aliasing of meridional gradients at MLO was a significant source of observed O_2 variability, and predicted that this effect would be greater at lower latitudes. The indication from Figs. 5–7, that selective sampling across the strong interhemispheric gradient was the source of the large variability in our measurements, confirms this prediction. These observations highlight the difficulty of measuring seasonal and interannual variations in low-latitude O_2 using background-station or shipboard flask measurements. Discrete samples taken at biweekly or monthly intervals could alias synoptic variations such as those presented here.

This month-long cruise coincided with the end of the largest El Niño event on record. At the midpoint of the cruise the sea surface temperature (SST) on the Equator at 140°W was 3 °C above average, at the end of the cruise it was average, and two weeks later it was 3 °C below average (TAO, 2002). This sudden collapse of the El Niño event requires a certain amount of caution in interpreting these coincident equatorial Pacific measurements. However, if the response of atmospheric gas concentrations to oceanic perturbations were slower than around one week, these measurements would represent close to full El Niño conditions. Dissolved O_2 measurements that we made on this cruise indicate that the eastern equatorial Pacific was consistently supersaturated during this time, and that this supersaturation was greater than that observed during previous El Niños (Stephens, 1999; Wanninkof et al., 1995). It was not possible to find any correspondence between observed small-scale dissolved and atmospheric O_2 variations. At least during this cruise, the equatorial O_2 source was too homgenous relative to the interhemispheric atmospheric gradient to imprint strong signals on the local atmosphere.

The implications of El Niño for our measured atmospheric O_2 and CO_2 concentrations are complex. During the initial stages of an El Niño a local O_2 outgassing, or reduced ingassing, may result from the decreased upwelling of O_2-depleted waters, followed at a slightly longer response time by an associated CO_2 ingassing signal. Eventually, however, as the broader equatorial Pacific region comes into equilibrium with the reduced input of preformed nutrients from below, an O_2 ingassing signal should result. Furthermore, the reduced air–sea heat flux in this region during El Niño will result in less outgassing of both O_2 and CO_2. Le Quéré et al. (2000) have investigated these effects using an equatorially enhanced version of the Océan Parallélisé (OPA) model run through 1997. This model qualitatively reproduces the timing of events outlined above for CO_2 (Le Quéré et al., 2000) and O_2 (C. Le Quéré, personal communication, 1999). Their results, when extrapolated to the time of this cruise and combined with an atmospheric transport model (Stephens, 1999) suggest that the atmospheric O_2 concentration we measured at the Equator was around 3 per meg lower than for average conditions. However, the fact that we measured ubiquitous surface water O_2 supersaturations suggests a differently timed response than in our extrapolation of the OPA results, and implies that our shipboard atmospheric O_2 observations may actually have been higher than they would have been during climatologically average conditions.

Another potentially significant El Niño influence on these observations is through altered wind patterns. Relative to the climatological mean, the winds on the Equator at 140°W were much more northerly and much less easterly during the 1997–98 El Niño event (TAO, 2002), which at the time of year of this cruise would have led to anomalously low O_2 concentrations. However, by the time of the cruise the wind had already returned to close to its normal velocity and direction, in advance of the SST shift (McPhaden, 1999; TAO, 2002). Future continuous shipboard O_2 measurements in the equatorial Pacific, in different phases of El Niño, would resolve many of these issues and provide new constraints on interannual biogeochemical responses in this region.

4. Shipboard measurements in the Southern Ocean

The Southern Ocean will play a critical role in the amount of anthropogenic CO_2 absorbed by the oceans in the coming decades, and this region may be particularly sensitive to potential future climate change (Sarmiento and Le Quéré, 1996). Despite a long recognition of the region's global importance, its harsh conditions have allowed only limited oceanographic and atmospheric observations, leaving much unknown about local biogeochemical processes and considerable uncertainty as to whether or not they are undergoing dramatic changes (Broecker et al., 1999). Flask samples collected at the South Pole (SPO) and Cape Grim, Tasmania (CGO) reveal much higher O_2 concentrations than predicted by coupled atmosphere–ocean carbon cycle models (Stephens et al., 1998). In addition, a comparison between these and other stations leads to the perplexing conclusion that annual-mean O_2 concentrations are higher at SPO than anywhere else on the globe, without any known annual-mean O_2 sources at high southern latitudes (Keeling et al., 1998a). Recent measurements in the Scripps O_2 Laboratory on flask samples from Palmer Station Antarctica (PSA) show O_2 concentrations that are much closer to the predictions of coupled ocean–atmosphere models (Stephens, 1999), but which make the annual-mean SPO values even harder to explain with a steady source–sink distribution. These measurements suggested that either the meridional O_2 gradients at high southern latitudes are much stronger than observed for other atmospheric species, or that some unknown systematic bias might be affecting the SPO flask measurements.

To address these growing questions, we used the VUV instrument to measure atmospheric O_2 in the Southern Ocean, aboard the NSF ship Lawrence M. Gould. The Lawrence M. Gould conducts research cruises throughout the Southern Ocean, but during the spring and fall of each year it makes several rapid transits from Punta Arenas, Chile to PSA in order to resupply the station and exchange personnel. Thus, similar to Ka'imimoana, this vessel provides an excellent opportunity for conducting atmospheric and oceanographic surveys that can be closely repeated in the future. The spring and fall also happen to be interesting times to measure atmospheric O_2 at these latitudes, as they correspond to the trough and peak of the relatively large O_2 seasonal cycle. The data presented here are from cruise leg 98-8A, the second resupply cruise of the austral spring, which left Punta Arenas on 27 September and returned on 8 October 1998. Because of a misrouting of equipment, we were only able to make measurements during the return leg (Fig. 8). Despite the shortened measurement period, the 7 d of data that we did obtain provide a good measure of the background atmospheric O_2 concentrations, and insights into the causes of their variability at these latitudes and this time of year.

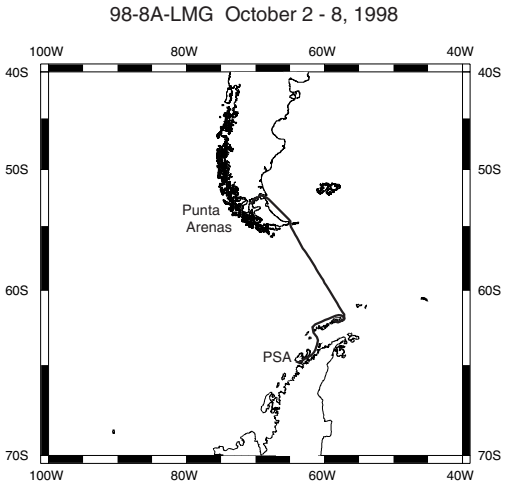

Fig. 8. Map showing the cruise track for the return leg of Lawrence M. Gould cruise 98-8A, which included a brief stop at King George Island.

The VUV O_2 and infrared CO_2 instruments analyzed air drawn from a bow mast on the ship, approximately 15 m above the water. A second, aft inlet was available; however, as the relative wind was always from the bow, this inlet was not used and stack air was only detected while the ship was on station. Figure 9 shows the measured O_2 and CO_2 concentrations presented as hourly mean values. The gap on 5 October represents data lost as a result of a power outage on the ship, and corresponds to a time period when the ship was offloading researchers and equipment at King George Island (Fig. 8). The vertical axes in this figure are scaled to be equal on a mole to mole basis, and it is clear that the O_2 variations are significantly greater than the CO_2 variations.

The most salient features in the O_2 data are (1) a gradual decreasing trend during the first day and a half with a total change of -25 per meg by early on 3 October, (2) a gradual rise and fall over the next 3 d,

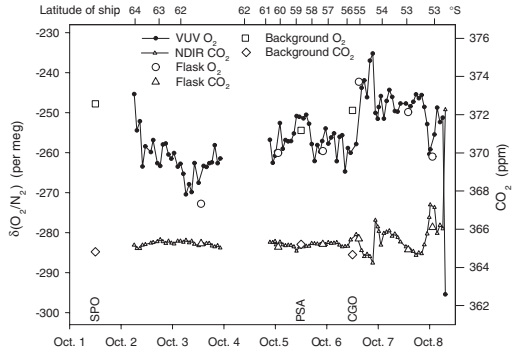

Fig. 9. Hourly-mean concentrations of atmospheric O_2 and CO_2 potted versus time, with the corresponding latitude indicated at the top of the plot, from 98-8A-LMG. The vertical axes are scaled to be equivalent on a molar basis. The uncertainties on the O_2 and CO_2 values are ± 3 per meg and ± 0.3 ppm, respectively. The ticks on the bottom *x*-axis correspond to midnight local time and are labeled with the date of the following day. The gap on 4 October corresponds to data lost during a ship power-outage. The large circles and triangles represent 5-L flask samples collected aboard the ship and analyzed on the Scripps interferometer. The large squares and diamonds represent flask trios collected at SPO (90°S) on 1 October, PSA (65°S) on 5 October and CGO (41°S) on 6 October as part of the Scripps O_2 Laboratory background sampling program. These background values are plotted at their time of sampling, but do not correspond to the shipboard latitude ticks on the upper scale.

upon which are superimposed shorter-term variations, (3) a step increase of 20 per meg in the afternoon of 6 October, followed by another 5 per meg jump and a 10 per meg drop later that evening, and (4) a brief dip down and up 15 per meg just before the end of the cruise. The CO_2 concentrations were very steady for the first 5 d of the cruise, though varying slightly in opposition to the O_2 variations. Beginning with the drop in O_2 and jump in CO_2 late on 6 October, the CO_2 variations were much larger than during the earlier period. The last point of very high CO_2 and very low O_2 was measured in the Straights of Magellan. It was clearly influenced by upwind fossil-fuel burning, and we include it in the analyses to help identify industrial signals in the earlier data.

The large symbols in Fig. 9 represent six flask samples that we collected on the ship and later analyzed on the Scripps O_2 Laboratory interferometer. The flask O_2 values are in good agreement with the proximate VUV measurements, and independently support the large positive and negative O_2 excursions observed by the VUV instrument on 6 October and early on 8 October, respectively. With the exception of an unexplained discrepancy with the last flask, the CO_2 values are also in good agreement. We have also included diamonds in Fig. 9 representing flask trios collected at SPO on 1 October, PSA on 5 October and CGO on 6 October as part of the Scripps O_2 Laboratory background sampling program. The O_2 and CO_2 concentrations we observed on 5 October are in good agreement with the PSA observations on the same day and 400 km to the south.

The observed relationships between the O_2 and CO_2 concentrations provide information, independent of any meteorological analyses, on the sources for the observed O_2 and CO_2 variations. Plotting O_2 versus CO_2 (Fig. 10) reveals a division of the data into two

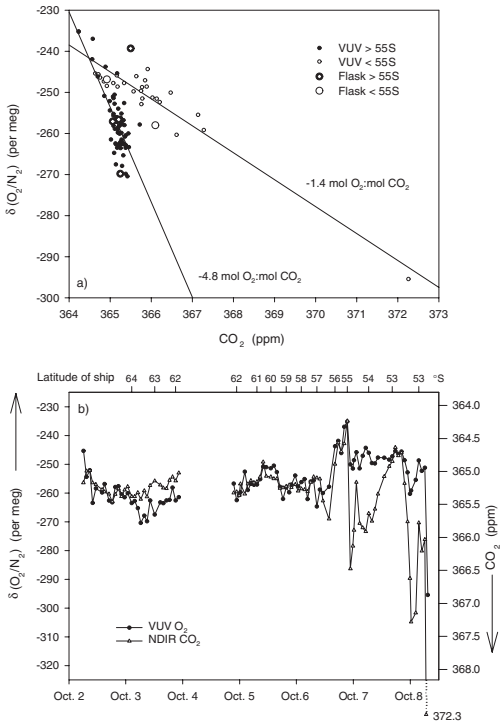

Fig. 10. (a) Hourly-mean and flask O_2 versus CO_2 concentrations from 98-8A-LMG. The lines and reported slopes are from least-squares fits to the VUV measurements made up to and including the maximum O_2 value at 55°S on 6 October (small filled circles) and including and after this point (small open circles). (b) Hourly-mean and flask O_2 and scaled CO_2 data. Same as Fig. 9, but with the CO_2 axis flipped and scaled by -4.8 mol O_2:mol CO_2.

modes. Up to and including the peak O_2 value late on 6 October, O_2 and CO_2 varied at an average ratio of -4.8 mol O_2:mol CO_2. In contrast, including and after the peak O_2 value, O_2 and CO_2 varied at an average ratio of -1.4 mol O_2:mol CO_2. The flask-station measurements shown in Fig. 9 indicate that the PSA O_2 concentration was lower and the PSA CO_2 concentration slightly higher than the respective concentrations at SPO and CGO. This was also the case in October of 1996 and 1997 (Stephens, 1999), and 1999–2001 (R. Keeling, unpublished data). The O_2:CO_2 ratio observed during the first part of this cruise of -4.8 is within the range of the flask-station gradient values observed at this time of year, and indicates that, similar to our equatorial data, the major source of O_2 variability was the result of sampling across the large-scale meridional O_2 gradient. The ratio of -1.4 observed during the last two and a half days of the cruise is very close to that expected from the combustion of liquid fossil fuels (Keeling, 1988). The division between these two periods is coincident with the passage of the ship into the lee of Tierra del Fuego, suggesting that the ship at this point began sampling air that had recently been influenced by industrial processes. The consistency of the O_2:CO_2 ratio as Punta Arenas was approached (Fig. 10a) confirms that anthropogenic emissions had the dominant influence on O_2 and CO_2 variability during this latter period.

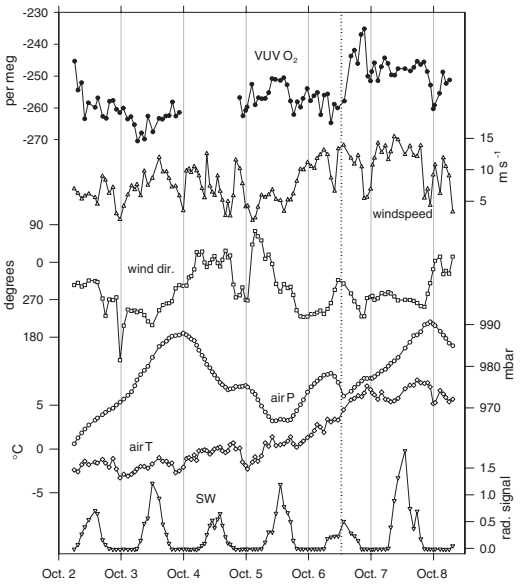

Fig. 11. Hourly-mean shipboard meteorological observations from 98-8A-LMG. The VUV O_2 data is the same as in Fig. 9. This plot also includes wind speed, wind direction, barometric pressure, air temperature and short-wave incoming radiation. Vertical reference lines are plotted every day at local midnight, and at 1248 local time on 6 October.

The large increase in O_2 on 6 October, however, does not appear to be an industrial signal, as it occurred some 5 h before the ship passed behind Tierra del Fuego, in the direction of higher not lower O_2, and at a molar ratio close to -5. Meteorological observations from this cruise provide some clues to the origin of this feature. Figure 11 shows the hourly-mean O_2 data plotted along with hourly-mean measurements of wind speed, wind direction, barometric pressure, air temperature and short-wave radiation. At the time of the 20 per meg O_2 jump, the wind was backing from the northwest to the southwest and the barometric pressure passed through a local nadir. This indicates that a center of low pressure passed eastward just to the south of the ship. The sharpness of the barometric pressure change, and the sudden decrease in cloud cover recorded by the short-wave radiometer, suggest that the ship may have passed through a front separating two distinct airmasses. Although the wind shifted to the south, it is possible that this newly sampled airmass had originally migrated from the north and had spent less time over the Southern Ocean than the previously sampled airmass. The fact that atmospheric temperature increased by 2–3 °C at this point supports this hypothesis.

Although back-trajectory analyses have the potential to clarify such issues, meteorological reanalyses may be subject to large uncertainties in this region, because of the lack of direct observations. Nonetheless, back-trajectory calculations (Stephens, 1999; Draxler and Hess, 1998) reflect the influence of a low pressure center to the south early on 6 October, as well as the passage of another low as the ship was moving up the Peninsula on 2 and 3 October. This earlier low resulted in a shift in the sampling of air from relatively far north to air from the south, which appears to correspond to the steady decrease in O_2 and increase in CO_2 observed during the first 2 d of measurements. Half of this 10 per meg drop in O_2 occurred while the ship was still on station at PSA, indicating a potential sensitivity to wind direction for the biweekly flask samples taken for O_2 analyses in the Scripps O_2 Laboratory.

Similarly, the gradual increase in O_2 on 5 October and decrease on 6 October appear to be associated with a shift in the origin of sampled air first to the north and then back to south, which can be seen in the measured

winds (Fig. 11). These features, and the sharp jump in O_2 on 6 October, occurred at similar ratios to CO_2. As the ship passed into the lee of Tierra del Fuego several hours after the 20 per meg O_2 increase, O_2 dropped and CO_2 jumped in proportion to the expected industrial O_2:CO_2 relationship. Less than 12 h later, CO_2 began a steady decrease, during which O_2 showed a small increase. These changes appear to suggest a temporary removal of the combustion signal, as they returned the O_2 and CO_2 concentrations to a point (left-most open circle in Fig. 10a) matching their earlier relationship. The CO_2 concentration increased again by the end of 7 October, and the variability during the remainder of the cruise was consistent with industrial forcing.

The zonal wind patterns at these latitudes lead to several convergences and divergences in the surface ocean (e.g. Tomczak and Godfrey, 1994). However, we did not observe any clear connections between local oceanographic properties and atmospheric concentrations (Stephens, 1999). This is not surprising, considering the relatively vigorous atmospheric mixing that was occurring. Although these measurements do not appear sensitive to local ocean variability, they do contain information on air–sea fluxes on larger scales. Furthermore, because of the relatively small terrestrial and industrial influences on background O_2 and CO_2 in this region, we can directly relate the O_2:CO_2 ratios from our observations south of Tierra del Fuego to ratios in air–sea fluxes. Consequently, such measurements provide a good opportunity for examining the predictions of ocean carbon cycle models and air–sea gas exchange climatologies.

Seasonal ocean carbon cycle models (Six and Maier-Reimer, 1996) and dissolved O_2 measurements (Najjar and Keeling, 1997; 2000) suggest strong uptake of O_2 over most of the Southern Ocean at this time of year. This ingassing of O_2 results from both biological and solubility forcing associated with the upwelling of O_2-depleted deep waters and cooling of the surface waters, respectively. For CO_2, these two influences are opposed because the upwelling deep water is enriched in inorganic carbon. We interpret our observed ratio of -4.8 mol O_2:mol CO_2 as an indication that for some upwind region the biological forcing was dominant and CO_2 was being emitted from the surface ocean. Although the biological imprint from respiration on the upwelling waters has a ratio of around -1.4 mol O_2:mol C, the buffering chemistry and relatively high solubility of CO_2 results in even greater air–sea fluxes for O_2 than for CO_2.

The spatial and temporal representativeness of this signal is somewhat uncertain. For example, the O_2:CO_2 ratio observed during this cruise could reflect large-scale gradients due to air–sea gas exchange over the whole Southern Ocean during the preceding several months, or regional gradients resulting from strong local variations in air–sea gas exchange during the preceding few days. A coupled ocean–atmosphere model with accurate winds would likely be necessary to refine this picture. Nonetheless, we know that strong zonal winds lead to rapid mixing at these latitudes and time of year. Because of this and the general agreement with O_2:CO_2 ratios from the multiyear October flask-station gradients we speculate that our observations indicate O_2 ingassing and CO_2 outgassing over a relatively large region of the Southern Ocean at the end of September and beginning of October.

The pCO_2 climatology compiled by Takahashi et al. (1999), with somewhat limited observations at high southern latitudes, shows net CO_2 uptake for the Southern Ocean in all months. However, this dataset also reveals a persistent region of high pCO_2 which extends south from the eastern equatorial Pacific to 50°S, about 30° west of South America. In austral spring, this region is joined by another relatively distinct patch of high pCO_2 surface water extending north from Antarctica about 40° west of Drake Passage. Such upwind areas of CO_2 outgassing may be responsible for the negative atmospheric O_2:CO_2 ratios we observed, and for the regionally high CO_2 concentrations at PSA at this time of year. The Hamburg Model of the Ocean Carbon Cycle, version 3.1 (Six and Maier-Reimer, 1996), similarly predicts net CO_2 uptake by the Southern Ocean with some opposing regions of outgassing during September and October. However, the areas predicted to be outgassing at this time of year by this model are all downwind of our measurements, in the Atlantic and Indian basins. When coupled to the TM2 atmospheric transport model (Heimann, 1995), the fluxes from this ocean model lead to positive correlations between O_2 and CO_2 at PSA at the time of our measurements (Stephens, 1999). Biological ocean general circulation models disagree markedly in the Southern Ocean (Stephens et al., 1998; Orr et al., 2001) and an error in the zonal location of CO_2 sources and sinks would not be surprising. Future high-resolution atmospheric O_2 and CO_2 measurements would help to improve our understanding of where and when biological, dynamic, and thermal processes influence Southern Ocean pCO_2.

Our shipboard observations appear to be in good agreement with the concurrent PSA samples (Fig. 9), and thus they suggest that the surprisingly low annual-mean atmospheric O_2 concentrations observed in PSA flask samples (Stephens, 1999) are not the result of a sampling artifact at this station. The strong meridional gradients observed in annual-mean O_2 at high southern latitudes may instead result in part from temporal correlations between atmospheric transport and surface fluxes. Such correlations can produce mean concentration gradients from balanced but varying fluxes, and are commonly known as rectifier effects in analogy to electronic rectifiers that convert an alternating current into a direct current (e.g. Denning et al., 1995; Stephens et al., 2000). Studies of the meteorology around SPO indicate the presence of a wintertime inversion over the South Pole which results from the strong radiative cooling of the surface in the absence of sunlight (e.g. Parish, 1988). Hogan et al. (1982) show that this inversion, as well as the katabatic influence of the polar high, work to isolate SPO from more northerly air for much of the winter season. This isolation can clearly be seen in the seasonal cycle of aerosols at SPO (Hogan et al., 1982; 1990; Samson et al., 1990). Because the time of isolation corresponds to O_2 uptake by the oceans around Antarctica, whereas the time of greater mixing corresponds to O_2 outgassing, there may be a net effect on the annual mean difference between SPO and PSA. In fact, flask observations show that the O_2 concentrations at these stations are very similar from November through February during the austral summer, but that the concentrations at PSA are systematically lower by about 15 per meg during the rest of the year (Stephens, 1999). Although rectifier effects can not be measured independently of net fluxes, it appears that this Antarctic seasonal O_2 rectifier effect may produce as much as a 10 per meg difference in annual-mean O_2 concentration between SPO and PSA.

Because of their coarse resolution, and the general lack of validation data for meteorological analyses over the Antarctic continent, global atmospheric transport models do not accurately represent the seasonality of horizontal and vertical transport to SPO. While this is not noticeable in the gases typically used to validate tracer transport models, as they do not have significant southern hemisphere sources, in the case of radon a wide range of models predict Antarctic seasonal cycles that are 180° out of phase with observations (Rasch et al., 2000). Not surprisingly then, the TM2 and TM3 atmospheric transport models predict positive rectifier gradients between PSA and SPO (Stephens et al., 1998), which are opposite to the indications from background flask samples. However, an incorrect Antarctic rectifier in the atmospheric transport model may not explain the interhemispheric model-observation discrepancies discussed by Stephens et al. (1998). A better representation of seasonal transport to SPO would likely improve the predicted SPO-PSA O_2 gradient, but it is unclear if it would do so by increasing the predicted annual-mean concentration at SPO or decreasing that at PSA. While the former would improve the match with observations, the latter would have a negative impact. Furthermore, this Antarctic rectifier effect is less likely to influence the modeled gradient between CGO and northern midlatitudes, which was also predicted to be much less than observed (Stephens et al., 1998). Future continuous shipboard O_2 measurements in the Southern Ocean, made at different times of year, would significantly improve our understanding of the present air–sea fluxes of carbon and oxygen in this region and the transport of their signals to background flask stations.

5. Concentration gradients between the equatorial Pacific and Southern Oceans

A distinct prediction of coupled ocean–atmosphere models is a strong gradient in annual-mean atmospheric O_2 decreasing from the Equator to high southern latitudes (Stephens et al., 1998; Aumont, 1998; Gruber et al., 2001). The measurements presented here may provide insight into the validity of this prediction. However, the brief temporal span of our measurements, the uncertainty concerning the influence of El Niño on our equatorial Pacific data, and the uncertainty concerning model representations of seasonal atmospheric mixing processes over Antarctica all limit the usefulness of this preliminary dataset in constraining coupled ocean–atmosphere models. Nonetheless, because we made these geographically distinct measurements with a single sampling and analytical system, they may provide a valuable check on conclusions drawn from flask samples which are subject to potential station-specific sampling biases. Thus, we present the absolute concentration differences here for purposes of comparison to existing and future measurements and models.

For simplicity, we have binned the equatorial Pacific and Southern Ocean data by even 5° latitude bands, and then calculated average times, positions

Table 1. *Values from both cruises separated in 5° latitude bins and averaged*

Date (year fract.)	Latitude (°N)	Longitude (°E)	O_2/N_2 (per meg, ±3)	CO_2 (ppm, ±0.3)	APO (per meg, ±3)	Hours of data
1998.38	17.45	−154.20	−253.5	369.70	−219.8	31
1998.38	11.86	−147.75	−252.9	369.67	−219.4	39
1998.37	7.34	−142.58	−240.7	368.68	−212.4	49
1998.35	2.41	−137.13	−235.2	367.95	−210.8	184
1998.35	−1.03	−139.69	−221.1	366.76	−202.8	36
1998.77	−53.45	−67.48	−249.7	365.70	−237.0	25
1998.77	−57.55	−62.18	−253.9	365.10	−244.4	23
1998.76	−62.98	−60.72	−259.7	365.22	−249.6	42

and concentrations for each bin. For the equatorial Pacific cruise, we have excluded all data before the fractionation problem was resolved on 30 April. For the Southern Ocean cruise, we have excluded the final data point in Fig. 9, which was clearly influenced by local industrial pollution. Table 1 shows the resulting average O_2 and CO_2 concentrations for both cruises. The standard errors of these mean values are significantly less than the accuracy estimates presented in section 2, so we use those larger error estimates here. In Table 1 we also present average values for the derived tracer atmospheric potential oxygen (APO) (Stephens et al., 1998). APO is a combination of O_2 and CO_2 concentration data that is essentially conservative with respect to terrestrial biotic processes, and is thus useful in constraining physical and biological oceanic processes. We calculate APO here according to

$$\mathrm{APO\,(per\,meg)} = \delta(O_2/N_2) + (CO_2 - 363.29) \times \frac{1.1}{X_{O_2}}. \quad (5)$$

This equation differs from that of Stephens et al. (1998) in that it does not include CO or CH_4 corrections, and it establishes an arbitrary CO_2 reference point that corresponds to the suite of calibration cylinders used to define zero on the Scripps O_2/N_2 scale.

The APO difference between 0–5°N in the middle of the Pacific in May and 60–65°S in Drake Passage in October of approximately −39 per meg results from a combination of annual-mean gradients and the strong seasonal uptake of O_2 occurring in Southern Hemisphere waters throughout the austral winter. Of the three models examined by Stephens et al. (1998), only the Hamburg Model of the Ocean Carbon Cycle, Version 3.1 (HAMOCC3.1) (Six and Maier-Reimer, 1996) has a seasonal cycle that can be compared to these data. When coupled to the TM2 atmospheric transport model, the HAMOCC3.1 model predicts within-region APO gradients that disagree somewhat with our observations (Stephens, 1999). However, this coupled model reproduces the large-scale observed difference between 0–5°N in the middle of the Pacific in May and 60–65°S in Drake Passage in October quite well, with a prediction of −37 per meg.

While this is certainly encouraging, we would also like to be able to investigate aspects of the ocean models, atmospheric models, and the data through annual-mean comparisons. Fortunately for our purposes, because the seasonal APO cycles are out of phase in either hemisphere, the seasonal amplitude near the Equator is quite small. Furthermore, the time of our equatorial Pacific cruise corresponded to a predicted zero crossing of this cycle. The HAMOCC3.1-TM2 model, which has been shown to reproduce seasonal APO cycles well in both the northern and southern hemispheres (Six and Maier-Reimer, 1996; Stephens et al., 1998), predicts that from 0–8°N at the longitude of our cruise the seasonal APO amplitude is only 15 per meg peak-to-peak and that at the time of our cruise the concentration was only 1.1 per meg higher than the annual-mean. Because of this predicted lack of seasonal influence, it is worth comparing our observations at this latitude with annual-means observed at nearby flask stations in the Scripps O_2 network. The annual-mean APO concentrations for Cape Kumukahi and American Samoa, centered on the time of our equatorial Pacific cruise, were −214.5 and −206.2 per meg, respectively. Our observed value of −210.8, from 0–5°N, lies directly between these values, and thus does not provide any evidence for the large annual-mean APO peak between these two stations predicted by annual-mean ocean models. As discussed by Stephens et al. (1998), a seasonal correlation between air–sea

fluxes and the movement of the ITCZ may explain much of this discrepancy.

For the Southern Ocean, the seasonal variability is too great to use our measurements to directly constrain annual-mean gradients. However, our Southern Ocean measurements do provide a valuable positive comparison to the PSA flask measurements, for which several years of data now exist. If we compare our 0–5°N equatorial Pacific measurements to the annual mean of PSA measurements centered on the time of this cruise, we get a southward-decreasing APO gradient of 3 per meg. By comparison, the predictions of this gradient by the coupled models in Stephens et al. (1998) range from 8 to 17 per meg. Potential causes for these discrepancies include (1) the influence of El Niño on our equatorial Pacific data (section 3), (2) errors in atmospheric model representations of seasonal mixing processes over Antarctica (section 4), (3) a lack of, or errors in, the seasonality of modeled air–sea fluxes and their interactions with the seasonal movement of the ITCZ (Stephens et al., 1998) and (4) an overestimation of O_2 and CO_2 ingassing at high southern latitudes and outgassing near the Equator. Clearly, additional measurements and modeling work will be required to resolve this picture further.

6. Conclusion

We have described the design and performance of a new instrument for measuring variations in atmospheric O_2. On land, this VUV instrument has a precision of 6 per meg O_2 at 10-s resolution and 1 per meg for a 5-min average, and it can be shipped easily between field sites. The motion-sensitivity characteristics of the instrument are good, and for typical conditions at sea these values only increased to 10 and 2.5 per meg for 10-s resolution and a 5-min average, respectively. The keys to attaining these high levels of precision are an optical source, signal detection, and signal amplification stable to near their theoretical limits, as well as a gas-handling system that can switch between two gases every 5 s with very small and short-lived pressure and flow perturbations. By comparison to flask and reference-cylinder concentrations determined by the Scripps O_2 Laboratory interferometer, we have shown that the external reproducibility of the VUV measurements is $\pm$ 3 per meg. As for any atmospheric O_2 instrument, the external reproducibility is potentially very sensitive to the gas-handling configuration. However, the design described here does not appear to suffer from fractionation problems. Further modifications to the instrument design presented here promise even greater performance. Recent tests using a commercially available sealed xenon lamp (Opthos, Rockville, MD), removing the beamsplitter and evacuated volume from the light path, improving the RF shielding, and switching more frequently have shown a factor of three improvement in short-term precision and elimination of the remaining motion sensitivity.

The atmospheric O_2 measurements presented here represent the first field-based measurements of atmospheric O_2 variations and the first *in situ* measurements of atmospheric O_2 in the equatorial Pacific and Southern Ocean regions. The results shown in Figs. 4–7 and Figs. 9–11 demonstrate that the shipboard VUV instrument is capable of detecting meaningful changes in atmospheric O_2 on time scales of hours to weeks and on space scales of tens to hundreds of kilometres. The comparisons with atmospheric CO_2 and meteorological measurements from our equatorial Pacific cruise (section 3) show that boreal-springtime equatorial atmospheric O_2 concentrations are strongly influenced by atmospheric mixing processes. As a result of the strong oceanic, terrestrial and industrial influences on the latitudinal gradients, O_2 concentrations were lower and CO_2 concentrations higher when the ship sampled air from further north. Likewise, we observed the highest O_2 and lowest CO_2 concentrations when the ship briefly sampled air that was primarily of southern hemisphere origin. Shipboard flask sampling programs promise many insights into global biogeochemical cycling. However, as noted above, flask samples taken near the Equator during spring and fall are likely to be highly variable due to selective sampling across the interhemispheric gradient. High-resolution continuous field-based measurements, such as the VUV measurements presented here, can provide additional information on the sources of O_2 variability and improved estimates of mean concentrations.

Measurements and meteorological analyses from our Southern Ocean cruise similarly show short-term variations that resulted from variations in the origin of the sampled air. Consistent with our understanding of austral-springtime processes, we measured significantly higher O_2 concentrations in air from more northern latitudes. The observed O_2:CO_2 ratio in these variations may represent the ratio between air–sea O_2 and CO_2 exchange integrated over several months and a relatively large area of the Southern Ocean, which would suggest the presence of a Southern Ocean source for CO_2 at this time of year. Ratios observed

later in the cruise appear to be consistent with and allow the identification of influences from industrial fossil-fuel combustion. The clean-air VUV O_2 measurements during this cruise were in good agreement with simultaneous flask samples collected onboard the ship and at Palmer Station, thus providing support for the VUV technique and for the surprisingly low O_2 values seen in the PSA flask record. As discussed in section 4, the significantly negative annual-mean O_2 gradient between SPO and PSA may be explained by a seasonal rectifier effect. The advantage of continuous measurements is further highlighted by the amount of information that is contained in this relatively short and highly variable time series.

We have reported average O_2 and CO_2 concentrations for each cruise corresponding to 5° latitude bins. Uncertainties associated with the effect of El Niño on equatorial atmospheric O_2 and CO_2 concentrations, as well as the strong seasonality in Southern Ocean atmospheric O_2, limit the ability of our measurements to constrain climatological-mean gradients. However, preliminary comparisons on the basis of the derived tracer APO do not show evidence for the equatorial peak or large decreasing gradient between equatorial and high-southern latitudes predicted by coupled ocean-atmosphere models. The predicted annual-mean gradients are likely sensitive to both the modeled annual-mean oceanic transport of CO_2 and O_2 and the seasonality of atmospheric mixing and air–sea fluxes near the Equator and Antarctica. Although many uncertainties remain, future measurements will make such comparisons more powerful. Initially resolving the influence of seasonal rectification effects on annual-mean concentrations will require repeated measurements at several different times of year. Then, rigidly constraining the oceanic transport of O_2 and CO_2, and quantifying its interannual variability, will require repeated measurements over several years.

The precision and portability of the VUV instrument lend it to a wide range of biogeochemical studies. Repeated ocean transects, similar to those presented here, can greatly increase the spatial resolution and extent of the current network of background O_2 measurements, which would improve our ability to partition terrestrial and oceanic CO_2 sources on global and hemispheric scales (Keeling et al., 1996). Shipboard atmospheric O_2 measurements over several years in the equatorial Pacific promise new insights into the biogeochemical responses to El Niño variability, while repeated measurements in the Southern Ocean would allow us to monitor biological and dynamical changes in a region that is expected to be particularly sensitive to future climate change. Another aspect of ocean geochemistry that the VUV instrument could address is improving theories and formulations for air–sea gas exchange. Eddy and gradient techniques for measuring air–sea CO_2 fluxes are continuously improving (McGillis et al., 2001; J. Smith, personal communication, 2002), and the VUV instrument could be applied to make complementary measurements of air–sea O_2 fluxes. Because O_2 and CO_2 have very different solubilities, measuring simultaneous fluxes of both gases would provide a new constraint on the solubility dependence of air–sea gas exchange.

The VUV instrument has a number of potential applications on land as well. Future VUV measurements from forest towers and *in situ* leaf and soil chambers could significantly advance our understanding of the relationships between plant O_2, CO_2 and nutrient cycling on a range of time and space scales. The VUV instrument could also be particularly helpful in determining net primary productivity at free-air carbon enrichment (FACE) sites. Because the intentional emission of CO_2 at these sites prevents the use of eddy-correlation CO_2-flux measurements, variations in productivity currently must be estimated by mass-balance techniques. Finally, the VUV instrument described here may also be suitable for airborne measurements. Because oceanic, terrestrial and industrial processes have inherently different O_2:CO_2 ratios, VUV measurements of vertical O_2 profiles would aid the interpretation of relative influences on CO_2. Separately identifying the terrestrial component of vertical and longitudinal CO_2 variations would help to constrain terrestrial rectification processes (Stephens et al., 2000), while using airborne VUV O_2 measurements to identify industrial contributions to CO_2 variations could prove valuable in future attempts at emission verification.

7. Acknowledgments

We thank NOAA, Richard Feely, Michael McPhaden, and the crew of the Ka'imimoana for their assistance in making the measurements presented in section 3, and NSF and crew of the Lawrence M. Gould for their assistance in making the measurements presented in section 4. Elizabeth McEvoy performed the flask analyses presented here and provided valuable laboratory assistance. We would like to thank Katharina Six and Ernst Maier-Reimer for providing

HAMOCC3.1 output, and Martin Heimann for providing the TM2 model. Terry Rawlins and Darin Toohey contributed to early instrumentation discussions. BBS was supported at the Scripps Institution of Oceanography by a NSF Graduate Research Fellowship and an Achievement Rewards for College Scientists Fellowship while conducting the research presented in this paper. This work was supported under NSF grants ATM-9612518 and ATM-0000923, DOE grant OE-FC03-90ER61010, and NOAA grant NA77RJ0453A. The National Center for Atmospheric Research is operated by the University Corporation for Atmospheric Research under sponsorship of the National Science Foundation.

REFERENCES

Aumont, O. 1998. Étude du cycle naturel du carbone dans un modèle 3D de l'océan mondial, Ph.D. Thesis, Univ. Pierre et Marie Curie, Paris.

Battle, M., Bender, M. L., Tans, P. P., White, J. W. C., Ellis, J. T., Conway, T. and Francey, R. J. 2000. Global carbon sinks and their variability inferred from atmospheric O_2 and ^{13}C. *Science* **287**, 2467–2470.

Bender, M. L., Tans, P. P., Ellis, J. T., Orchardo, J. and Habfast, K. 1994. A high precision ratio mass spectrometry method for measuring the O_2/N_2 ratio of air, *Geochim. Cosmochim. Acta* **58**, 4751–4758.

Bender, M. L., Ellis, J. T., Tans, P. P., Francey, R. and Lowe, D. 1996. Variability in the O_2/N_2 ratio of Southern Hemisphere air, 1991–1994: Implications for the carbon cycle. *Global Biogeochem. Cycles* **10**, 9–21.

Broecker, W. S., Sutherland, S., and Peng, T.-H. 1999. A possible 20th-century slowdown of Southern Ocean deep water formation. *Science* **286**, 1132–1135.

Denning, A. S., Fung, I. Y. and Randall, D. A. 1995. Latitudinal gradient of atmospheric CO_2 due to seasonal exchange with land biota. *Nature* **376**, 240–243.

Draxler, R. R. and Hess, G. D. 1998. An overview of the HYSPLIT_4 modelling system for trajectories, dispersion, and deposition. *Aust. Meteorol. Mag.* **47**, 295–308.

Gruber, N., Gloor, M., Fan, S.-M. and Sarmiento, J. L. 2001. Air–sea flux of oxygen estimated from bulk data: Implications for the marine and atmospheric oxygen cycles. *Global Biogeochem Cycles* **15**, 783–804.

Heimann, M. 1995. The global atmospheric tracer model TM2. *Tech. Rep. 10*, Deutsch. Klimarechenzentrum, Hamburg, Germany, 53 pp.

Hogan, A., Barnard, S., Samson, J. and Winters, W. 1982. The transport of heat, water vapor and particulate material to the South Polar Plateau. *J. Geophys. Res.* **87**, 4287–4292.

Hogan, A. W., Egan, W. G., Sampson, J. A., Barnard, S. C., Riley, D. M. and Murphey, B. B. 1990. Seasonal variation of some constituents of Antarctic tropospheric air. *Geophys. Res. Lett.* **17**, 2365–2368.

Inn, E. C. Y., Watanabe, K. and Zelikoff, M. 1953. Absorption coefficients of gases in the vacuum ultraviolet. Part III. CO_2, *J. Chem. Phys.* **21**, 1648–1650.

IPCC 2001. *Climate Change 2001: The Scientific Basis. Contribution of Working Group I to the Third Assessment Report of the Intergovernmental Panel on Climate Change* (eds. J. T. Houghton et al.). Cambridge Univ. Press, New York.

Kaplan, A., Jurgens, C. and Yu, K. 1971. Ultraviolet oxygen sensor, *Instrument and Control Systems*, February, 113–114.

Keeling, R. F. 1988. Development of an interferometric oxygen analyzer for precise measurement of the atmospheric O_2 mole fraction, Ph.D. Thesis, Harvard Univ., Cambridge, Mass, 178 pp.

Keeling, R. F. and Shertz, S. R. 1992. Seasonal and interannual variations in atmospheric oxygen and implications for the global carbon cycle. *Nature* **358**, 723–727.

Keeling, R. F., Najjar, R. G., Bender, M. L. and Tans, P. P. 1993. What atmospheric oxygen measurements can tell us about the global carbon cycle. *Global Biogeochem. Cycles* **7**, 37–67.

Keeling, R. F., Piper, S. C. and Heimann, M. 1996. Global and hemispheric CO_2 sinks deduced from changes in atmospheric O_2 concentration. *Nature* **381**, 218–221.

Keeling, R. F., Manning, A. C., McEvoy, E. M. and Shertz, S. R. 1998a. Methods for measuring changes in atmospheric O_2 concentration and their application in southern hemisphere air. *J. Geophys. Res.* **103**, 3381–3397.

Keeling, R. F., Stephens, B. B., Najjar, R. G., Doney, S. C., Archer, D. and Heimann, M. 1998b. Seasonal variations in the atmospheric O_2/N_2 ratio in relation to the kinetics of air–sea gas exchange. *Global Biogeochem. Cycles* **12**, 141–163.

Kronick, M. N., Bryson, C. E., Bridgham, J. A. and Eletr, S. H. 1980. Measurement of oxygen by differential absorption of UV radiation. U.S. Patent No. 4192996.

Le Quéré, C., Orr, J. C., Monfray, P., Aumont, O. and Madec, G. 2000. Interannual variability of the oceanic sink of CO_2 from 1979 to 1997. *Global Biogeochem. Cycles* **14**, 1247–1265.

Manning, A. C. 2001. Temporal variability of atmospheric oxygen from both continuous measurements and a flask sampling network: Tools for studying the global carbon cycle, Ph.D. thesis, University of California, San Diego, CA, 202 pp.

Manning, A. C. and Keeling, R. F. 1994. Correlations in short-term variations in atmospheric oxygen and carbon dioxide at Mauna Loa Observatory., In *Climate Monitoring and Diagnostics Laboratory No. 22 Summary Report* (ed. J. T. Peterson). NOAA ERL, Boulder, CO, 121–123.

Manning, A. C., Keeling, R. F. and Severinghaus, J. P. 1999. Precise atmospheric oxygen measurements with a paramagnetic oxygen analyzer. *Global Biogeochem. Cycles* **13**, 1107–1115.

McGillis, W. R., Edson, J. B., Hare, J. E. and Fairall, C. W. 2001. Direct covariance air–sea CO_2 fluxes. *J. Geophys. Res.* **106**, 16,729–16,746.

McPhaden, M. J. 1999. Genesis and evolution of the 1997–1998 El Niño. *Science* **283**, 950–954.

Najjar, R. G. and Keeling, R. F. 1997. Analysis of the mean annual cycle of the dissolved oxygen anomaly in the World Ocean. *J. Marine Res.* **55**, 117–151.

Najjar, R. G. and Keeling, R. F. 2000. Mean annual cycle of the air–sea oxygen flux; a global view. *Global Biogeochem. Cycles* **14**, 573–584.

Orr, J. C., Maier-Reimer, E., Mikolajewicz, U., Monfray, P., Sarmiento, J. L. and coauthors, 2001. Estimates of anthropogenic carbon uptake from four three-dimensional ocean models. *Global Biogeochem. Cycles* **15**, 43–60.

Parish, T. R. 1988. Surface winds over the Antarctic continent: A review. *Rev. Geophys.* **26**, 169–180.

Rasch, P. J., Feichter, J., Law, K., Mahowald, N., Penner, J. and coauthors. 2000. A comparison of scavenging and deposition processes in global models: results from the WCRP Cambridge Workshop of 1995. *Tellus* **52B**, 1025–1056.

Samson, J. A. R. 1967. *Techniques of vacuum ultraviolet spectroscopy*, Wiley, New York, 348 pp.

Samson, J. A., Barnard, S. C., Obremski, J. S., Riley, D. C., Black, J. J. and Hogan, A. W. 1990. On the systematic variation in surface aerosol concentration at the South Pole. *Atmos. Res.* **25**, 385–396.

Sarmiento, J. L. and Le Quéré, C. 1996. Oceanic carbon dioxide uptake in a model of century-scale global warming, *Science* **274**, 1346–1350.

Severinghaus, J. P. 1995. Studies of the terrestrial O_2 and carbon cycles in sand dune gases and in Biosphere 2. Ph.D. Thesis, Columbia Univ., New York, 148 pp.

Six, K. and Maier-Reimer, E. 1996. Effects of plankton dynamics on carbon fluxes in an ocean general circulation model. *Global Biogeochem. Cycles* **10**, 559–583.

Stephens, B. B. 1999. Field-based atmospheric oxygen measurements and the ocean carbon cycle. Ph.D. Thesis, University of California, San Diego, 221 pp.

Stephens, B. B., Keeling, R. F., Heimann, M., Six, K. D., Murnane, R. and Caldeira, K. 1998. Testing global ocean carbon cycle models using measurements of atmospheric O_2 and CO_2 concentration. *Global Biogeochem. Cycles* **12**, 213–230.

Stephens, B. B., Wofsy, S. C., Keeling, R. F., Tans, P. P. and Potosnak, M. J. 2000. The CO_2 Budget and Rectification Airborne Study: Strategies for measuring rectifiers and regional fluxes. *Inverse Methods in Global Biogeochemical Cycles*, Geophysical Monograph 114, AGU.

Stephens, B., Bakwin, P., Tans, P. and Teclaw, R. 2001, Measurements of atmospheric O_2 variations at the WLEF talltower site, Sixth International Carbon Dioxide Conference, Extended Abstracts, Vol. I, [Nakazawa, T.], Tohoku Univ., Sendai, 78–80.

Takahashi, T., Wanninkhof, R. H., Feely, R. A., Weiss, R. F., Chipman, D. W., Bates, N., Olafsson, J., Sabine, C. and Sutherland, S. C. 1999. Net sea–air CO_2 flux over the global oceans; An improved estimate based on the sea-air pCO_2 difference. In *Proceedings of the 2nd International Symposium CO_2 in the Oceans* (ed. Y. Nojiri). Center for Global Environmental Research, Japan, 9–15.

TAO 2002. The Tropical Atmosphere Ocean Array. http://www.pmel.noaa.gov/tao, NOAA Pacific Marine Environmental Laboratory, Seattle.

Tohjima, Y. 2000. Method for measuring changes in the atmospheric O_2/N_2 ratio by a gas chromatograph equipped with a thermal conductivity detector. *J. Geophys. Res.* **105**, 14,575–14,584.

Tomczak, M. and Godfrey, J. S. 1994. *Regional oceanography: an iIntroduction*. Pergamon, Oxford, 67–87.

Wanninkhof, R., Feely, R. A., Atwood, D. K., Berberian, G., Wilson, D., Murphy, P. P. and Lamb, M. F. 1995. Seasonal and lateral variations in carbon chemistry of surface water in the eastern equatorial Pacific during 1992. *Deep-Sea Res. II* **42**, 387–409.

Watanabe, K., Inn, E. C. Y. and Zelikoff, M. 1953. Absorption coefficients of oxygen in the vacuum ultraviolet. *J. Chem. Phys.* **21**, 1026–30.

Wong, J. Y. 1978. Measuring gaseous oxygen with U.V. absorption. U.S. Patent 4096388.

Wong, J. Y. 1986. Oxygen analysis employing absorption spectroscopy. U.S. Patent 4591721.